Evaluation of the DNA Binding Tendencies of the Transition State Regulator AbrB†

Benjamin G. Bobay,‡ Linda Benson,§ Stephen Naylor,§,|| Brett Feeney,‡ A. Clay Clark,‡ Michael B. Goshe,‡ Mark A. Strauch,⊥ Richele Thompson,‡ and John Cavanagh*,‡

Department of Molecular and Structural Biochemistry, North Carolina State University, Raleigh, North Carolina 27695, Biomedical Mass Spectrometry and Functional Proteomics Facility, Department of Biochemistry and Molecular Biology, Mayo Clinic/Foundation, Rochester, Minnesota 55905, and Biomedical Sciences Department, Dental School, University of Maryland at Baltimore, 666 West Baltimore Street, Baltimore, Maryland 21201

Received July 27, 2004; Revised Manuscript Received October 5, 2004

ABSTRACT: Global transition state regulator proteins represent one of the most diverse classes of prokaryotic transcription factors. One such transition state regulator, AbrB from *Bacillus subtilis*, is known to bind more than 60 gene targets yet displays specificity within this target set by binding each promoter with a different affinity. Microelectrospray ionization mass spectrometry (μESI-MS), circular dichroism, fluorescence, UV spectroscopy, and molecular modeling were used to elucidate differences among AbrB, DNA, and AbrB−DNA complexes. μESI-MS analysis of AbrB confirmed its stable macromolecular state as being tetrameric and verified the same stoichiometric state in complex with DNA targets. μESI-MS, circular dichroism, and fluorescence provided relative binding affinities for AbrB−DNA interactions in a qualitative manner. UV spectroscopy was used in a quantitative manner to determine solution phase dissociation constants for AbrB−DNA complexes. General DNA structural parameters for all known natural AbrB binding sequences were also studied and significant similarities in topological constraints (stretch, opening, and propeller twist) were observed. It is likely that these parameters contribute to the differential binding proclivities of AbrB. In addition to providing an improved understanding of transition state regulator−DNA binding properties and structural tendencies of target promoters, this comprehensive and corroborative spectroscopic study endorses the use of μESI-MS for rapidly ascertaining qualitative binding trends in noncovalent systems in a high-throughput manner.

The key to bacterial adaptability and survival lies in the organism's capacity to initiate an appropriate response for a specific environmental situation. These situations include changes in chemical concentrations, temperature, osmolarity, viscosity, light, pH, density, and exposure to anti-infectives. Accordingly, bacterial responses also comprise numerous forms, ranging from the secretion of toxins, polymer-degrading enzymes, and antibiotic synthesis to the organism undergoing complete physiological transformation. In this final case, many bacteria can undergo cellular differentiation leading to the development of endospores which are highly resistant to heat, sunlight, chemicals, and drugs (*1*).

Bacteria do not make these decisions frivolously. Instead, they enter a cellular holding pattern termed the "transition state" to consider whether a measured protective response is required. During such periods of critical decision making, the responsibility of channeling the cell along the proper pathway falls to a class of transcriptional regulators termed transition state regulator proteins (*2*−*4*). The role of a transition state regulator is multifaceted, assisting the cell as it constantly evaluates the surroundings while also ensuring that cellular processes required for both growth and survival are regulated simultaneously through the activation of normally silent genes (*2*, *5*−*7*). Since bacterial environments are in constant flux, it is likely that bacteria spend much of their time in this state. As more genomes are sequenced, the prevalence of transition state regulator proteins is becoming more apparent. More than 30 known or potential global transition state regulators of the antibiotic resistance protein B (AbrB)[1] class are present in *Bacillus*, *Clostridium*, *Carboxydothermus*, *Geobacillus*, *Listeria*, *Oceanobacillus*, *Pyrococcus*, *Pasteuria*, *Staphylococcus*, *Streptococcus*, *Sulfolobus*, and *Thermoanaerobacter* (*8*, *9*). This rapidly expanding list of AbrB-like transition state regulators reinforces the importance of determining both the general and specific mechanisms of AbrB−DNA binding.

The only transition state regulator to have been characterized to any extent is AbrB from *Bacillus subtilis* (*7*, *10*−*14*). AbrB has recently been identified as a regulator of the lethal factor, edema factor, and protective antigen toxins in *Bacillus anthracis*, the causative agent in anthrax infection (*15*, *16*). AbrB regulates, with high affinity, the expression

† This work was supported by NIH Grants RO1 GM55769 (to J.C.) and R01 GM46700 (to M.A.S.), the Kenan Institute for Engineering, Technology and Science (J.C.), and the Mayo Foundation (S.N.).

* To whom correspondence should be addressed. Telephone: (919) 513-4349. Fax: (919) 515-2047. E-mail: john_cavanagh@ncsu.edu.

‡ North Carolina State University.

§ Mayo Clinic/Foundation.

|| Current address: Division of Biological Engineering, Room 56-738, Massachusetts Institute of Technology, Cambridge, MA 02139.

⊥ University of Maryland at Baltimore.

[1] Abbreviations: AbrB, antibiotic resistance protein B; AbrBN, antibiotic resistance protein B residues 1−53; ΔAbs, change in absorbance; ΔAbs_{total}, change in absorbance total; K_d, dissociation constant; μESI-MS, microelectrospray ionization mass spectrometry; SELC, size exclusion liquid chromatography.

10.1021/bi048399h CCC: $27.50
Published on Web 11/26/2004

Table 1: DNA Sequences Used in All Bioanalytical Studies

promoter	sequence (5′−3′)[a]
sinIR	CTA GAT TTA ATG GCA AAT GAC TTC CAG AGA
spo0E	CTA GAA TAT GTT TAC AAA TAA AGT ATA ATC TGT AAT AAT GCA C
BS18	CAA CAA ATT GGA AAA CAT TGC CAG TAG AAA GCA CTA GCG AAC TA
TGGNA3	AAA TTG GAA AAC ATT GCC AGT AGA AAA ATT GGA AAA CAT TGC CAG TAG AA
TGGNA1	TAT GGG AGT TAT ACC ATG TTT TAT GGG AGT TAT ACC ATC TTT
negative control	TAC TAC TGC TGA GCC CGG TAC TTA CTG CTG AGC CCG G

[a] The 5′−3′ sequences of DNA used in μESI-MS, CD, fluorescence, UV, and modeling studies.

of more than 60 different genes nominally expressed or repressed in suboptimal environments. Among the functions it regulates during the transition state are transport systems for sugars, antibiotic synthesis, degradative enzymes, regulation of the phosphate regulon, oxidative/osmotic stress functions, cell division regulators, histidine and nitrate utilization enzymes, protein secretion, and regulators of cellular differentiation, including sporulation. Particularly striking is the fact that the DNA sites targeted by AbrB share no apparent consensus sequence. Although our investigations of the DNA-binding domain of AbrB (residues 1−53, AbrBN) have aided in the understanding of these promiscuous DNA recognition properties, the model is still incomplete (*9*, *17*). While AbrB has broad DNA binding properties, it does exhibit specificity. Certainly it does not bind randomly to DNA (*18*, *19*). Additionally, AbrB does not bind to all its cognate promoters with the same affinity, implying another level of discrimination. Affinity constants for AbrB binding to several promoters have been determined through filter binding and gel retardation assays with reported K_d values varying greatly (*2*−*4*, *18*, *20*−*24*). While these techniques provide a good approximation for affinity, filter binding and gel retardation assays require separation of bound and free mixture components for analysis and can perturb the equilibrium position (*25*, *26*).

In this study, AbrB's DNA binding preferences were investigated using microelectrospray ionization mass spectrometry (μESI-MS) in a rapid manner to determine relative binding affinities. μESI-MS provided unique insights into the regulation of these DNA targets, so much so that a variety of bioanalytical and computational techniques were used to further investigate and validate the μESI-MS findings. A more quantitative analysis of the dissociation constants of these AbrB−DNA complexes was then provided by solution phase UV spectroscopy. Additionally, the DNA targets were further characterized using circular dichroism (CD), tyrosine fluorescence emission spectrophotometry, and molecular modeling. These complementary studies were carried out in an effort to evaluate DNA characteristics that may contribute to the binding specificity as seen in μESI-MS. These data represent the first comprehensive attempts to assess such specific properties for this system. Our analysis reinforces the hypothesis that AbrB−DNA interactions are strongly dependent upon the topological structure of the particular DNA sequence and/or its propensity to adopt a suitable conformation. Furthermore, all the spectroscopic techniques that have been employed disclose the same protein−DNA binding hierarchy that was initially observed via μESI-MS. This is a particularly important point since it validates μESI-MS as a particularly attractive and efficient method for rapidly generating accurate *relative* binding affinities for protein−DNA interactions in a high-throughput manner.

EXPERIMENTAL PROCEDURES

Construction of the pET21b-AbrB Construct. The constructed plasmid and purified protein corresponding to full-length AbrB were obtained from DNA fragments (via PCR methods) using oligonucleotide primer pairs AbrB-Forward and AbrB-Reverse: AbrB-Forward, 5′-CAG GAA A**CA TAT G**AA ATC TAC TGG-3′; AbrB-Reverse, 5′-GAG AGT A**GG CGG** TTT TGA AGC-3′.

Primers were designed to incorporate NdeI and EcoRI restriction sites. These fragments were inserted into the pET21b expression vector from Novagene to place the genes under isopropyl β-D-thiogalactopyranoside (IPTG) inducible transcription. DNA sequencing confirmed that the desired constructs were obtained. The expression plasmids were introduced into *Escherichia coli* cells [Bl(21)DE3 cell line], and transformants were tested for IPTG-induced overexpression of polypeptides of the desired size (ca. 10 500 Da). All transformants that were tested exhibited induction of an ∼10−11 kDa protein.

Expression and Purification of AbrB and AbrBN. Expression and purification of AbrB and AbrBN were carried out as previously described by Benson et al. (*19*). Briefly, expression was carried out in the Bl(21)DE3 cell line and purification through Q-Sepharose and heparin columns. Purification was monitored throughout with 12% tricine gel electrophoresis.

DNA. All oligonucleotides and their complementary strands were synthesized by MWG Biotech, Inc., or the Molecular Biology Core Facility at the Mayo Clinic/Foundation. These sequences are shown in Table 1. Oligonucleotides were annealed in 100 mM NH_4HCO_3 (pH 8.0) in a heating block set at 95 °C for 10 min and gradually cooled to room temperature. Concentrations of double-stranded oligonucleotides used in this study were obtained from using extinction coefficients and serial dilutions and confirmed via UV spectroscopy.

Microelectrospray Ionization Mass Spectrometry. μESI-MS was carried out as previously described (*8*, *19*). Briefly, stock protein solutions in 10 mM Tris-HCl (pH 8.3 at 4 °C or pH 7.9 at room temperature), 1 mM EDTA, 0.1 mM $MgCl_2$, and 10 mM KCl were exchanged into 10 mM NH_4HCO_3 (pH 8.0) using a P-6 gel filtration spin column (Bio-Rad, Hercules, CA). Ammonium bicarbonate-buffered AbrBN and AbrB proteins were diluted to 40 and 30 μM, respectively, and infused into the μESI source at 0.3 μL/min. All protein−DNA complexes were combined at a 2:1 protein:DNA ratio (40 μM AbrBN with 20 μM DNA or 30 μM AbrB with 15 μM DNA) and incubated at room temperature for 45−60 min prior to μESI-MS analysis.

Circular Dichroism. CD spectra were measured using a Jasco J600A spectropolarimeter using a 0.1 cm (far-UV)

Table 2: Known Natural AbrB DNA Targets Used in Modeling Studies[a] in Addition to Those Listed in Table 1

promoters	regulation[b]	absolute position[c]	location	target binding sequence	ref
abrB	negative	45219−45248	−43:−14	CAAAATGATTGACGATTATTGGAAACCTTG	*23*
aprE	negative	1105085−1105157	−59:+15	AAAATCATCTCAAAAAAATGGGTCTACTAAAATATT ATTCCATCTATTACAATAAATTCACAGAATAGTCTTT	*23*
bsuB1	ND	ND	−60:−10	GAAAAGTACCAGCAGGGTTTATTGTGTT --AATCATTACAAAAAATGATAAA	*22*
comK	negative	1116464−1116583	ND	CATTAAATATCATTAAAAGATGATTTTATCTT AAATGTTAAAAAAACCTGTCGTTTTACAAAAA CAGATGATAGATTATTAGTATAAATTTTGCAG AAAAAGGATGGAGGCCATAATATG	*14*
dppA	negative	1359815−1359848	−16:+18	TTTAATATAATTTGTTAGAATATTCATAATTTAG	*24*
ftsA	negative	1595731−1595749	−1:+18	AATAAACATAAAATGTGAA	*22*
ftsA	negative	1595765−1595788	+34:+57	TTCTGTTGTTATTTTTTGTTACAC	*22*
hutP	positive	4040438−4040460	+199:+221	CAATTGAAACCGCTTCCAAAAAG	*2*
kinB	negative	ND	−20:ND	AAAATGAAGATTATAAATCACAATATTAT	*22*
pbpE	negative	3534606−3534630	−75:ND	ATGTGATGGGTTAAAAAGGATCTCT	*22*
pbpE	negative	3534573−3534598	−40:ND	GGATTTTTCAAAATATTTGAAACGTT	*22*
rbsR	positive	3700294−3700370	−133:−67	GAAATCTTCATCCATATTTGTGAAGACTTTGTC AAAAAAAGAGTGAAAACCTTAAATTTTTCAA TTATATATACAAT	*18*
rbsR	positive	3700432−3700464	−4:+29	CTATGTAAACGGTTACATAAACAAGGAGGAGCT	*18*
sigW	negative	194824−194850	+14:+41	GAGGTTAGATAAATATGGAAATGATGA	*13*
sinI	negative	2551623−2551645	+24:+46	TTTAATGGCAAATGACTTCCAGA	*12*
sinI	negative	2551622−2551647	ND	ATTTAATGGCAAATGACTTCCAGAGA	*21*
spo0E	negative	1430061−1430095	−39:−5	TATGTTTACAAATAAAGTATAATCTGTAATAATGC	*23*
spo0H	negative	116537−116576	−35:+5	TGACGCTTTTTTGCCCAATACTGTATAATATTTCTA TCTA	*22*
spoVG	negative	55753−55822	−75:−6	TAACTATATCCTATTTTTTCAAAAAATATTTTAAAAA CGAGCAGGATTTCAGAAAAAATCGTGGAATTGA	*4*
tycA	negative	ND	−60:−35	TTTTTTGCAAAATATCCCTATTTTTTAAT	*4*
tycA	negative	ND	+169:+199	GAAGGGAATTTCCCAGAAACAGGAAATTTTCT	*4*
tycA	negative	ND	+207:+231	TTAAAATACCCAAATGATGGAAAAT	*4*

[a] From http://dbtbs.hgc.jp/COG/tfac/AbrB.html. [b] Positive regulation (upregulation), negative regulation (downregulation), and ND (unknown). [c] Reference in this paper.

Hellma cuvette (Hellma Corp.). All measurements were corrected for background signal, and buffer conditions were subtracted under the same experimental conditions. For the protein−DNA complex, protein spectra were subtracted under the same experimental conditions, leaving spectral contributions of solely the DNA. All protein−DNA complexes were combined at a 2:1 protein:DNA ratio (15 μM AbrBN with 7.5 μM DNA or 15 μM AbrB with 7.5 μM DNA) and incubated at 4 °C for 24 h. Stock protein and DNA were stored in 10 mM Tris-HCl (pH 7.5), 10 mM KCl, 1 mM EDTA, and 1 mM DTT and/or 10 mM NH_4HCO_3 (pH 8.0). Spectra were collected for both types of buffering conditions. Titrations were performed with $MgCl_2$ at 0.2 μM to 0.2 mM. Spectra were recorded in triplicate at 25 ± 1.0 °C from 190 to 320 nm.

Tyrosine Fluorescence Emission. Tyrosine fluorescence emission measurements were performed using a PTI C-61 spectrofluorometer (Photon Technology International) with a 1 mL four-sided Hellma cuvette (Hellma Corp.). Samples were excited at 275 nm (tyrosine fluorescence), and emission was measured from 300 to 400 nm. Protein and protein−DNA spectra were collected in triplicate at 10 mM Tris-HCl (pH 7.5), 10 mM KCl, 1 mM EDTA, and 1 mM DTT and/or 10 mM NH_4HCO_3 (pH 8.0). All protein−DNA complexes were formed using a 2:1 protein:DNA ratio (15 μM AbrBN with 7.5 μM DNA or 15 μM AbrB with 7.5 μM DNA) and incubated at 4 °C for 24 h. pH titrations were completed in triplicate at 10 mM Tris-HCl, 10 mM KCl, 1 mM EDTA, and 1 mM DTT at varying pHs (6.0−8.5). The instrument was equipped with thermostated cell holders, and the temperature was held constant at 25 ± 1.0 °C using a circulating water bath.

UV Spectroscopy. Spectrophotometric binding studies were performed using an Agilent 8453 UV−vis spectrophotometer (Agilent Technologies Inc., Palo Alto, CA). Protein−DNA binding was monitored by measuring the absorbance between 190 and 1100 nm in a 1 cm, 25 μL quartz Hellma cuvette (Hellma Corp.). Changes in spectral features due to DNA−protein binding were identified by subtraction of protein spectra, resulting in only DNA contributions being present. Concentrations of protein to be titrated ranged 1 order of magnitude on either side of the previously reported or expected K_d for that particular DNA target, and DNA concentrations were kept at the previously reported or expected K_d. Six sets of scans were taken, and dissociation constants were calculated from the average of these scans. Changes in absorbance for each scan and normalization to the DNA concentration at 260 nm provided the data points for K_d determination. The resulting graphs were then fit to eq 1:

$$\Delta Abs/\Delta Abs_{total} = [ligand]_{total}/(K_d + [ligand]_{total}) \quad (1)$$

where ΔAbs is the observed change in absorbance from 200 to 240 nm, ΔAbs_{total} is the difference in ΔAbs from the first titration point to the last measurement point, and $[ligand]_{total}$ is the concentration of the protein at a particular measurement point.

Molecular Modeling. DNA sequences used in modeling studies are outlined in Table 2 in addition to those in Table 1. DNA Protein Data Bank files were constructed with

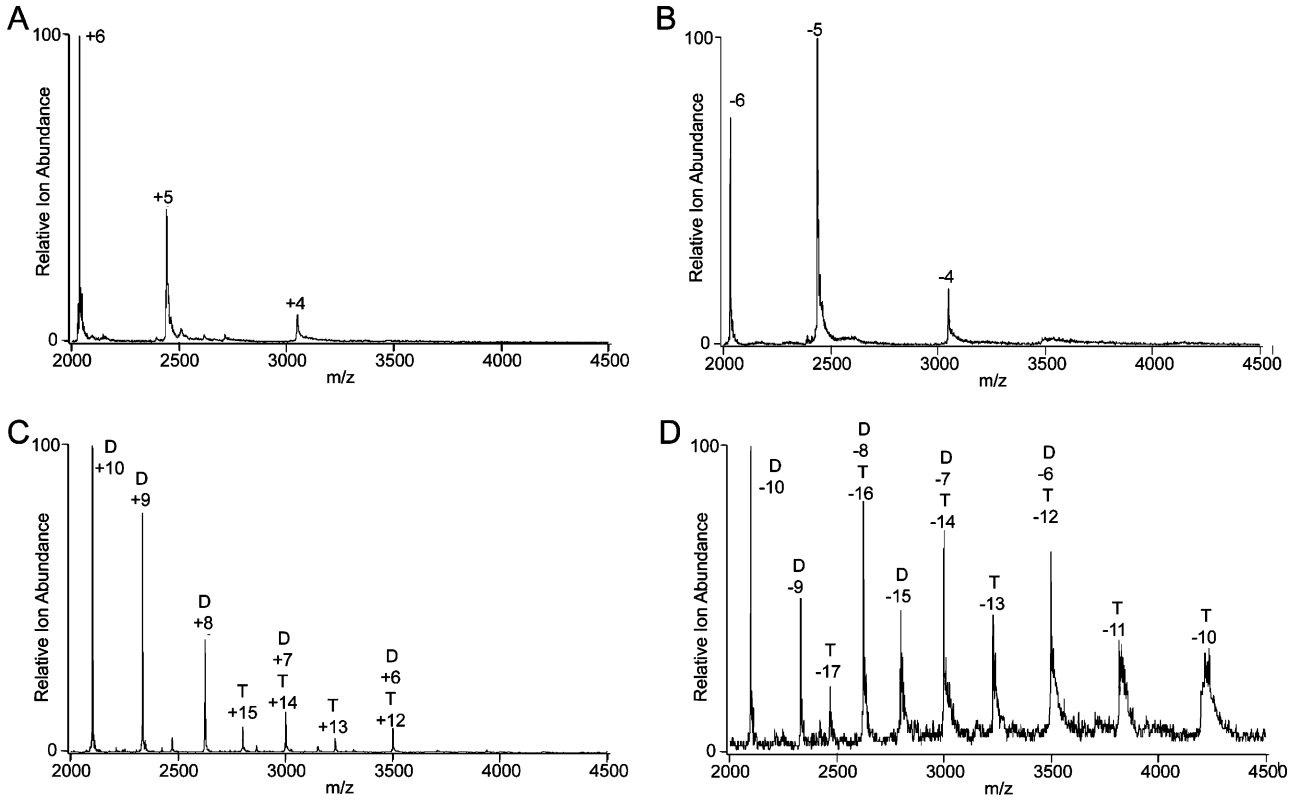

FIGURE 1: μESI mass spectrum of AbrB and AbrBN. Positive and negative ion spectra of 40 μM AbrBN and 30 μM AbrB in 10 mM ammonium bicarbonate buffer (pH 8.0). Peaks marked with a D or T correspond to dimeric or tetrameric species, respectively, with the indicated charge states: (A) positive ion spectrum of AbrBN, (B) negative ion spectrum of AbrBN, (C) positive ion spectrum of AbrB, and (D) negative ion spectrum of AbrB. Any peaks labeled with an M in panels A−D and any peak labeled with a D in panels C and D are artifacts of the ESI-MS process (see the text for a discussion).

MODEL IT (http://hydra.icgeb.trieste.it/~kristian/dna/) (*27*). MODEL IT was used to construct straight B-DNA and bent B-DNA in a 2 and 3 bp step. Helical parameters were obtained from running all of the PDB entries (four PDB entries per sequence) obtained from MODEL IT, with AMBER minimizations, through the program 3DNA (*28*).

RESULTS

Microelectrospray Mass Spectrometry. Figure 1A shows the positive ion mode μESI-MS spectrum of AbrBN. The charge state envelope (*m*/*z* 2000−3000) includes both monomeric and dimeric species. Monomeric AbrBN shows a charge state range of +4 to +6, which deconvolutes to a molecular mass of 6098 Da (expected mass of 6100 Da). Monomeric AbrBN has previously been shown to be an expected artifact of the transition from the liquid to gas phases during the μESI-MS process (*8*, *19*, *29*). Size exclusion liquid chromatography (SELC) and native gel electrophoresis have shown only dimeric AbrBN is present in solution; therefore, no monomeric−dimeric equilibrium exists (*19*, *21*, *30*). Dimeric AbrBN shows a charge state series of +4 to +5 which deconvolutes to a molecular mass of 12 196 Da (expected mass of 12 198 Da). Figure 1B shows the negative ion mode μESI-MS spectra of AbrBN. This spectrum affords the same molecular masses as the positive ion mode spectrum upon deconvolution.

The multimeric state of wild-type AbrB was also examined using μESI-MS and reveals a population of monomeric, dimeric, and tetrameric species, as shown in panels C and D of Figure 1. Monomeric and dimeric AbrB have previously been shown to be expected artifacts of the transition from the liquid to gas phase during the μESI-MS process (*8*, *19*, *29*). SELC and native gel electrophoresis have shown that only tetrameric AbrB is present in solution; therefore, no monomeric−dimeric−tetrameric equilibrium exists (*19*, *21*, *30*). The charge state envelope ranges from *m*/*z* 2000 to 3500 and is composed of charge states of +6 to +10 for the dimeric species ("D") and +12 to +15 for the tetramer ("T") (Figure 1C). Deconvolution of peaks corresponding to tetramers provides a molecular mass of 41 972 Da (expected mass of 41 976 Da). The same multimeric states were observed for AbrB in the negative ion mode (Figure 1D). The tetramer is the highest-order multimeric form of AbrB observed.

Figure 2 shows the negative ion mode μESI-MS spectra resulting from the incubation and subsequent complexation of AbrB with a series of target DNA sequences in a 2:1 ratio. Figure 2A shows spectra of the AbrB−*sinIR* complex, Figure 2B spectra of the AbrB−*spo0E* complex, Figure 2C spectra of the AbrB−*BS18* complex, and Figure 2D spectra of only the AbrB protein, which, though incubated with the negative DNA control, was unable to form a complex with it. Figure 3 shows the negative ion mode μESI-MS spectra resulting from the incubation and subsequent complexation of AbrBN with the same series of targets in a 2:1 ratio. Figure 3A shows spectra of the AbrBN−*sinIR* complex, Figure 3B spectra of the AbrBN−*spo0E* complex, Figure 3C spectra of the AbrBN−*BS18* complex, and Figure 3D spectra of only AbrBN, which, though incubated with the negative DNA control, was unable to form a complex with it. The AbrB−

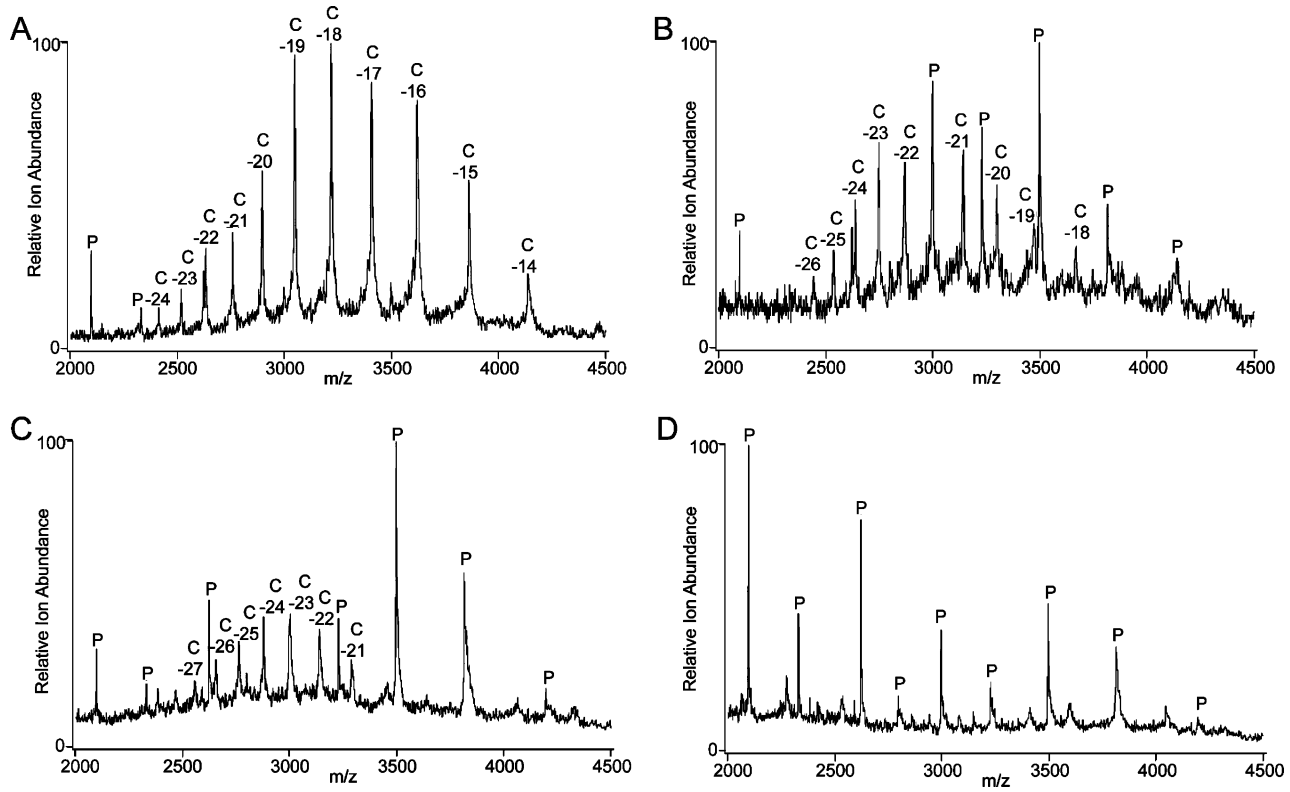

FIGURE 2: μESI mass spectrum of AbrB incubated with the target DNA sequences. Negative ion spectrum of 40 μM AbrB incubated with each DNA target sequence at 20 μM: (A) *sinIR*, (B) *spo0E*, (C) *BS18*, and (D) negative control oligonucleotides. Peaks marked with a C correspond to fully complexed tetrameric AbrB and DNA (no peaks corresponding to the monomer or dimer protein are observed); broad peaks in the baseline correspond to unbound DNA, while peaks marked with a P correspond to unbound protein, with the indicated charge states (see the text for a discussion).

sinIR and AbrBN−*sinIR* complexes provided a molecular mass consistent with tetrameric AbrB and dimeric AbrBN binding to one DNA molecule, and there are no other multimeric states observed in complex with DNA targets (*8*, *19*, *31*). These same stoichiometries of binding are observed for *all* detectable protein−DNA complexes examined using μESI-MS with the exception of the negative control DNA, for which no binding was observed. Examining the relative intensities of complex peaks to unbound protein and DNA and taking ionization efficiencies into account (see the Discussion), we rapidly ascertained the following hierarchy of relative binding affinities: *sinIR* ≫ *spo0E* > *BS18* > *TGGNA3* > *TGGNA1* ≫ negative control (no binding). Data are not shown for TGGNA3 and TGGNA1.

Circular Dichroism. One of the best means of measuring DNA distortion due to protein binding is via CD spectroscopy. CD spectra of double-stranded DNA are dominated by nearest-neighbor base interactions, which are highly sensitive to the distance and orientation of the neighboring bases (*32*). CD of AbrB and AbrBN was monitored in the far-UV spectrum. Far-UV analysis of AbrB and AbrBN furnishes spectra that are consistent with a protein with characteristics of both α-helix and β-sheet, with two unequal minima at approximately 208 and 219 nm (data not shown). Figure 4 shows the results from CD studies of DNA alone and of AbrB− and AbrBN−DNA complexes. All wavelength scans were performed from 190 to 320 nm. Figure 4A shows data for DNA only, with Figure 4B as an expansion of the 200−230 nm region. Maxima and minima at 275 and 245 nm, respectively, indicate a B-DNA structure (*33*). The structure of the DNA was significantly influenced upon binding AbrBN (Figure 4C,D) and AbrB (Figure 4E,F). Intensities changed across the entire spectrum, but when the reaction was monitored at ∼215 nm (maximum for *sinIR*), a recognizable trend for protein−DNA binding was discernible. A DNA distortion difference plot (the difference in intensity at ∼215 nm for each oligonucleotide from the intensity of the negative control in its unbound and bound state) showed the same hierarchy of binding as seen in the μESI-MS studies (Figure 5; see the Discussion). The relative changes in intensity at ∼215 nm upon AbrB and AbrBN binding rank the DNA: *sinIR* ≫ *spo0E* > *BS18* > *TGGNA3* > *TGGNA1* ≫ negative control (no binding) (the same order seen in μESI-MS). CD experiments were performed in the same buffer as the μESI-MS studies, as well as in Tris buffer, to make certain no contributions to binding or conformational changes were induced by the buffer. Furthermore, all CD experiments were performed with and without $MgCl_2$ to ensure no ionic cofactor was required for binding; in both instances, no differences in the spectra were observed (data not shown).

Tyrosine Fluorescence Emission Spectrophotometry. AbrB has two tyrosine residues, at positions 37 and 48, both in the N-terminal DNA-binding domain. The protein has no phenylalanine or tryptophan residues. Tyrosine fluorescence emission spectra following excitation at 275 nm are superimposable for each protein for the pH range from 6.0 to 8.5 (Figure 6A). To confirm no factor is needed for or induces changes in conformation or binding, $MgCl_2$ (0.100 μM to 0.200 mM) titrations in ammonium bicarbonate and Tris buffer were investigated. The titrations showed no difference in spectra, congruent with CD titrations (data not shown).

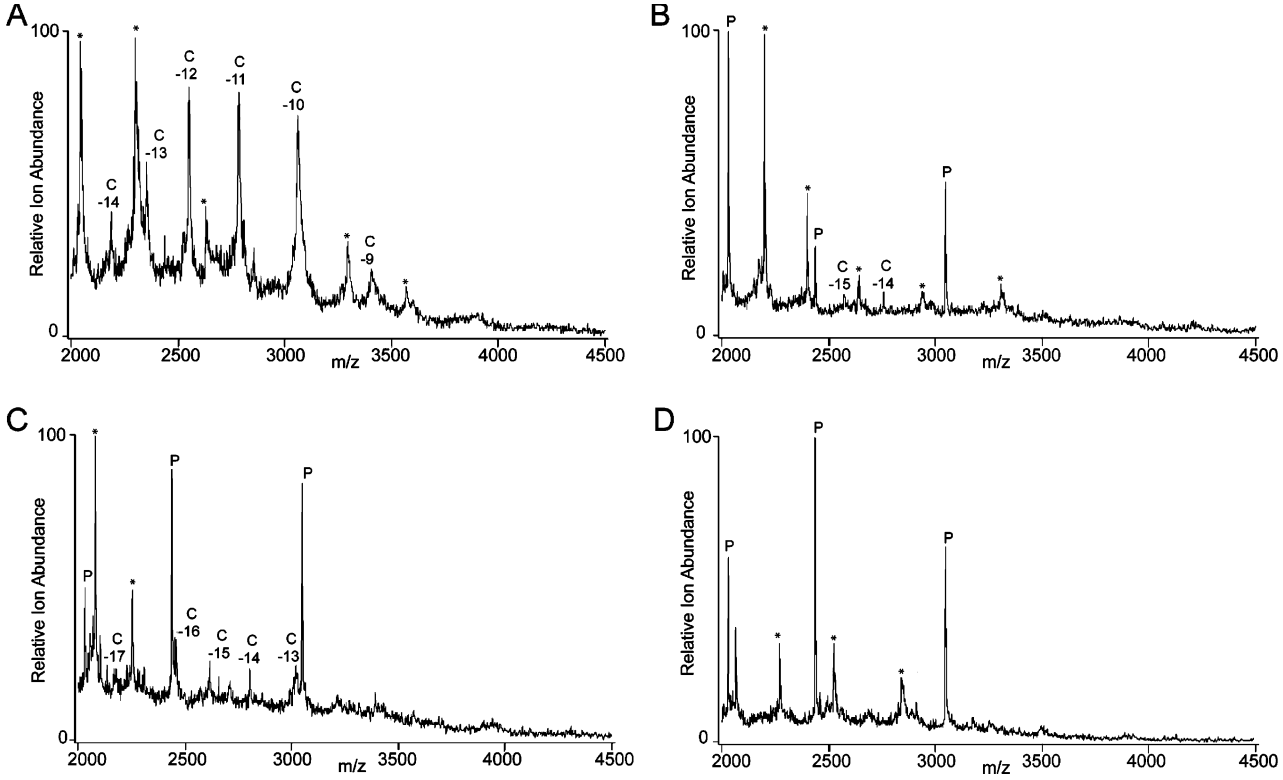

FIGURE 3: μESI mass spectrum of AbrBN incubated with the target DNA sequences. Negative ion spectrum of 30 μM AbrBN incubated with each DNA target sequence at 15 μM: (A) *sinIR*, (B) *spo0E*, (C) *BS18*, and (D) negative control oligonucleotides. Peaks marked with a C correspond to fully complexed dimeric AbrBN and DNA (no peaks corresponding to the monomer or dimer protein are observed); peaks marked with an asterisk correspond to unbound DNA, while peaks marked with a P correspond to unbound protein, with the indicated charge states (see the text for a discussion).

Relative fluorescence levels decrease approximately 2-fold (2.0×10^6 to 1.0×10^6) for AbrB compared to AbrBN.

Fluorescence emission spectra for the DNA titrations were similar for both AbrB and AbrBN protein samples. The greatest disparity between the relative fluorescence curves for the AbrB−DNA complex in Figure 6A is seen at ~345 nm. Since μESI-MS and CD both demonstrated that *sinIR* was the strongest binder of AbrB, normalization of the intensity of the fluorescence spectra at 345 nm with respect to *sinIR* revealed the same relative affinity order of binding for AbrB and AbrBN. Therefore, a strength-of-interaction hierarchy identical to that observed in the μESI-MS and CD studies is seen at 345 nm in the fluorescence emission study (Figure 6B). This trend is as follows: *sinIR* ≫ *spo0E* > *BS18* > *TGGNA3* > *TGGNA1* ≫ negative control (no binding).

UV Spectroscopy. UV spectroscopy was used to clarify previously reported dissociation constants for AbrB−DNA complexes (*3*, *18*, *34*); however, this study identified the K_d values in a solution phase manner. These K_d values are listed in Table 3 along with previously reported affinity constants (*3*, *18*, *34*). Scanning from 190 to 1100 nm allowed for the determination of binding trends in the titration of DNA with protein. Dissociation constants were determined by varying the protein concentration while holding the DNA concentration constant. Due to spectral dominance by the protein, K_d determinations were limited by the ability to observe structural changes solely attributed to the DNA. Because of this, trends were observed for only three of the six DNA targets. Changes in absorbance, as seen in Figure 7, were then fit to eq 1, and the dissociation constants were determined by averaging over six titration scans. The general trend observed for AbrB−DNA binding was the same as seen for μESI-MS, CD, and fluorescence.

DNA Modeling. It is likely that the specificity of AbrB binding is related to a particular DNA topology (*18*, *22*). To investigate if known natural AbrB binding targets might exhibit any shared topological characteristics distinct from DNA sequences not bound by AbrB, specific helical parameters of the target sites were modeled using 3DNA (*28*). 3DNA, a program capable of handling complex algorithms for the analysis, reconstruction, and visualization of three-dimensional nucleic acid structures, was used to accurately define local DNA structure. Table 4 lists the modeled parameters of intrinsic DNA topology pertaining to AbrB binding and recognition. Minor groove width, propeller twist, opening, stretch, and other structural parameters were examined. Rotational structural components of DNA are described by the parameters propeller twist and opening. Propeller twist is the angle of rotation between adjacent nucleotides in the non-nucleotide plane. Opening is the angle in adjacent nucleotides in the nucleotide plane. The translational structural component of DNA is represented by the parameter stretch, the distance between adjacent nucleotides.

Plots of propeller twist versus opening, opening versus stretch, and propeller twist versus stretch display a linear relationship (Figure 8), suggesting a close correlation of these parameters. In addition, all the natural binding sequences analyzed here, along with *BS18, TGGNA1*, and *TGGNA3*, are clustered within a distinct region in each case (boxed in Figure 8; Tables 1 and 2). The single outlier in each case is the negative control DNA. The requirements for acceptable

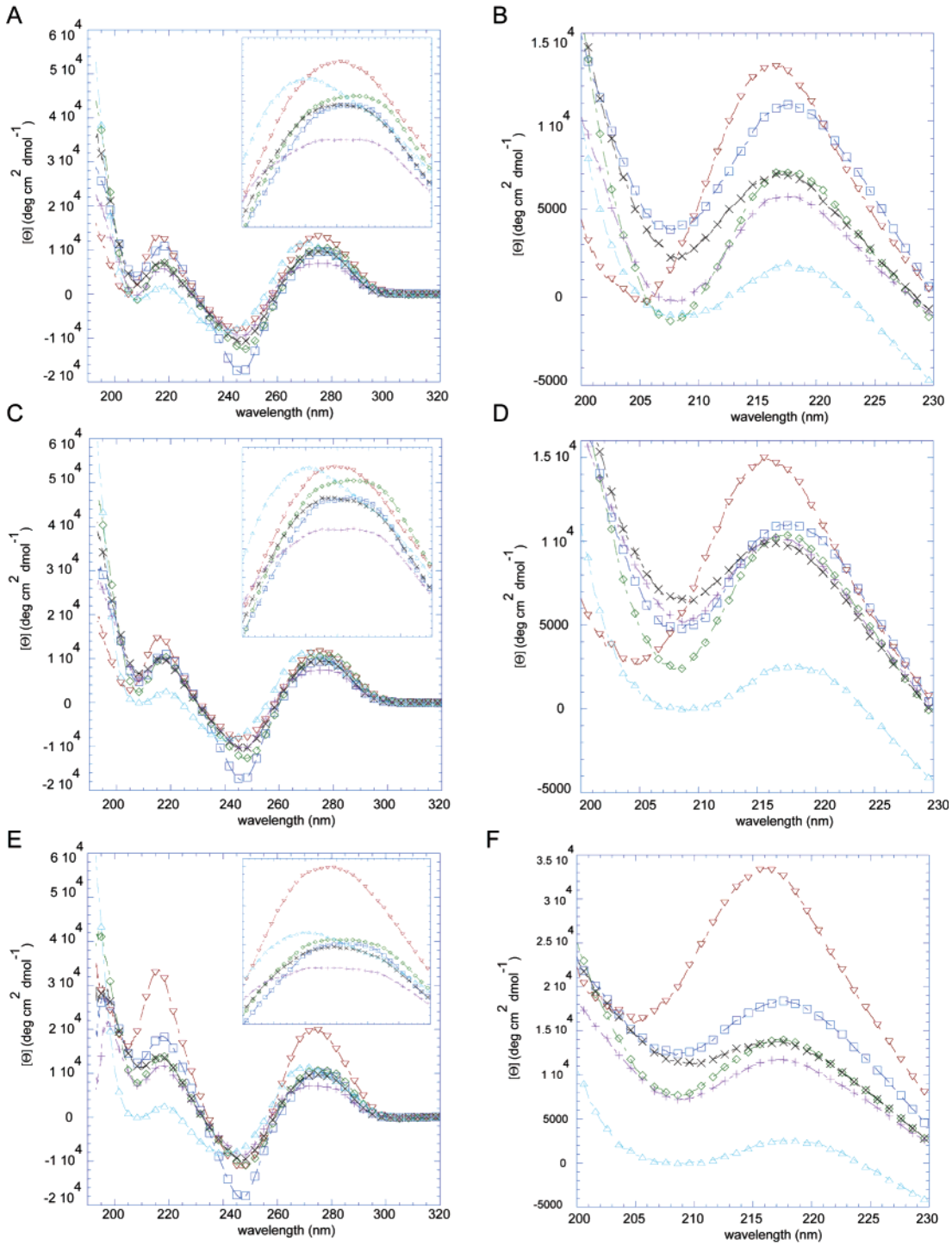

FIGURE 4: Near- and far-UV circular dichroism spectra of DNA and protein−DNA complexes. Protein:DNA ratio of 2:1 (same as μESI-MS): red ▽, *sinIR*; blue □, *spo0E*; green ◇, *BS18*; black ×, *TGGNA3*; pink +, *TGGNA1*; and cyan △, negative control. (A and B) DNA only, (C and D) AbrBN−DNA complex; and (E and F) AbrBN−DNA complex. All spectra have protein contribution subtracted out. All scans were from 190 to 320 nm with the inset from 260 to 290 nm.

values of propeller, opening, and stretch are −0.108° to −0.087°, −6.32° to −7.18°, and 0.132−0.172°, respectively. Distances calculated for one turn of B-DNA suggested a length of approximately 26.4−30.36 Å for all oligonucleotides that were examined, including the negative control. However, comparison of the minor groove distances reveals a width of approximately 4.6−7.4 Å for all oligonucleotides which bind AbrB. The negative control has a minor groove width of only 4.0 Å, lying outside of the range of appropriate values for the minor groove widths for establishing a binding interaction.

DISCUSSION

AbrB regulates the expression of more than 60 different genes nominally expressed or repressed in suboptimal environments. The genes are regulated to different extents, and the AbrB-binding sites responsible for regulation exhibit no apparent consensus base sequence linking them. Although

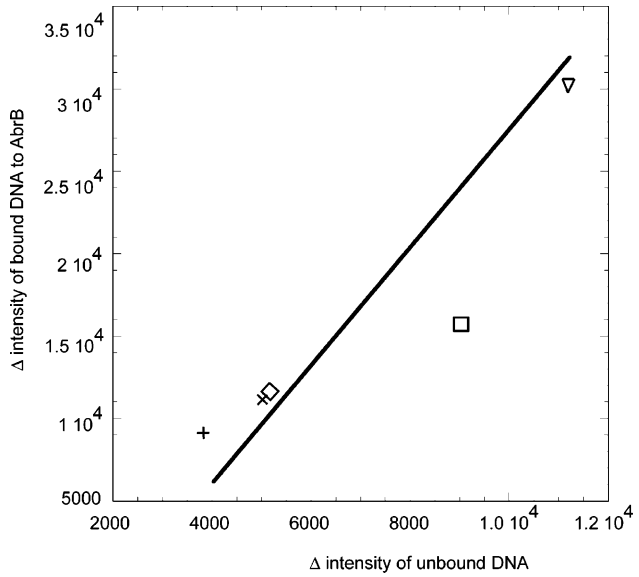

FIGURE 5: DNA distortion difference plot of AbrB−DNA CD data. Data obtained from subtraction of the maximum intensities around ~215 nm for each oligonucleotide from the intensity of the negative control in its unbound and bound state. The *Y*-axis is the difference in intensity of the AbrB titrations. The *X*-axis is the difference in intensity of the unbound DNA: (▽) *sinIR*, (□) *spo0E*, (◇) *BS18*, (×) *TGGNA3*, (+) *TGGNA1*, and (△) negative control. The resulting order of the strength of DNA distortion is the same as the relative binding affinity seen in the μESI-MS studies.

initial investigations of the DNA-binding domain of AbrB have aided in the understanding of these promiscuous DNA recognition properties, there is still much that is unknown (*9*, *17*). At this time, the most detailed mechanism proposed for describing DNA targeting by AbrB is simply that the protein appears to recognize some general DNA tertiary structure (*8*, *17*, *22*, *30*, *35*). From DNase 1 footprinting assays, it is known that AbrB binds to one face of the DNA with a coverage length equal to the width of one turn of DNA or longer, suggesting at minimum an interaction between the protein and DNA in the major and minor grooves (*3*, *21*). The studies described in this work represent the first attempts to expand on these original observations and/or hypotheses and to provide more detailed information about the general AbrB−DNA interaction.

The DNA target sequences used in this study were chosen for several reasons: *sinIR* and *spo0E* are well-studied AbrB-binding sites present in *B. subtilis* promoters (*3*, *18*, *34*, *36*). *BS18* was chosen because it contains one "idealized" AbrB binding sequence of TGGNA-5 bp-TGGNA; *TGGNA1*, *TGGNA3*, and the negative control were constructed on the basis of results from Strauch et al. (*3*). The negative control was designed to represent an area known to be completely unprotected in DNase 1 footprinting assays, not just from sequences that exhibited weak, sub-millimolar binding (*3*). To further elucidate the mode of interaction, μESI-MS experiments were performed on AbrB, AbrBN, and protein−DNA complexes.

Our initial goal was to identify a rapid, but accurate, method for determining the relative binding affinities of AbrB for different gene targets. With this in mind, we explored the use of μESI-MS for efficiently measuring the relative strength of the AbrB−DNA noncovalent interaction. μESI-MS studies were performed at 10 mM NH_4HCO_3 (pH 8.0)

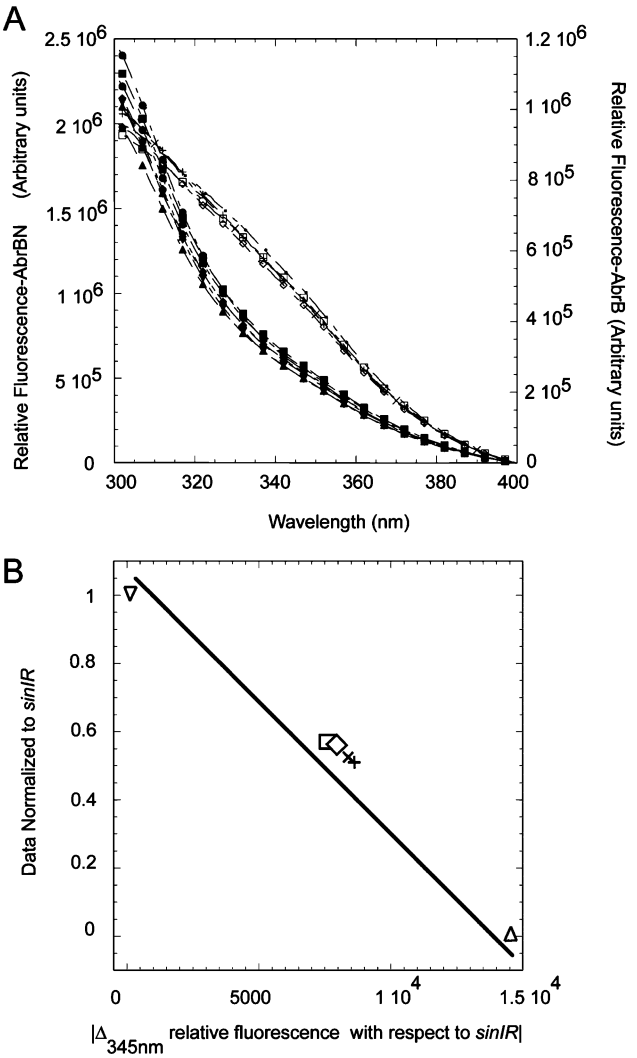

FIGURE 6: Tyrosine fluorescence emission spectrum of AbrB and AbrBN. Experiments were performed in 10 mM Tris-HCl, 10 mM KCl, 1 mM EDTA, and 1 mM DTT or 10 mM NH_4HCO_3 at varying pH (6.0−8.5). (A) In the double-*y*-axis plot (the left axis corresponds to AbrBN with filled symbols and the right axis corresponds to AbrB with the empty symbols) are depicted the results of a pH titration study on the protein. (B) Protein difference plot of AbrB binding to DNA, with the data normalized to *sinIR*'s intensity: (▽) *sinIR*, (□) *spo0E*, (◇) *BS18*, (×) *TGGNA3*, (+) *TGGNA1*, and (△) negative control. The resulting graph conveys the same relative order as seen in μESI-MS.

Table 3: Comparison of Dissociation Constants for AbrB−DNA Interactions Obtained Using UV Spectroscopy (this work) with Previously Determined Dissociation Constants[a]

promoter	K_d[b] (nM)	K_d[c] (nM)	K_d[d] (nM)	K_d[e] (nM)
sinIR	0.75 ± 0.15	−	−	28−200
spo0E	3.3 ± 0.90	300	−	6−23
BS18	>40	30	4	−
TGGNA 3	N/D[f]	−	−	−
TGGNA 1	N/D[f]	−	−	−
negative control	−	−	−	−

[a] Solution phase K_d determination was accomplished to clarify previous reports of gel shift assay measurements that may have had the equilibrium process perturbed by separation of bound and free components. [b] From this work. [c] From ref *34*. [d] From ref *3*. [e] From ref *21*. [f] Could not be experimentally determined using UV spectroscopy.

to preserve multimeric protein complexes and to examine formation of complexes between AbrB or AbrBN and known natural binding promoters. The experiments were performed

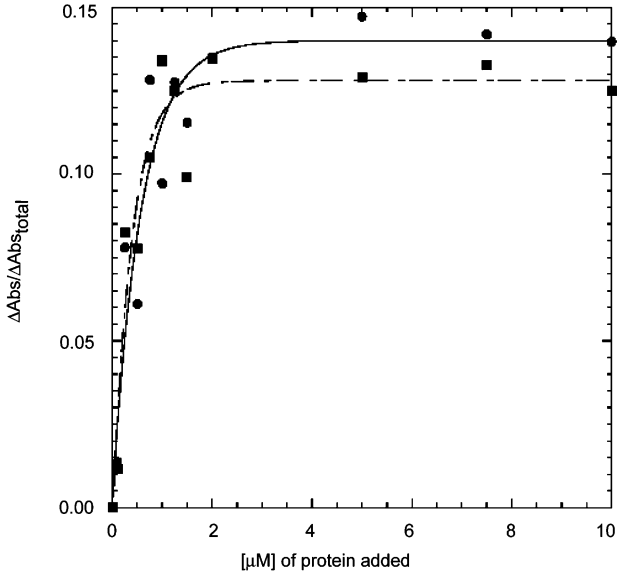

FIGURE 7: UV spectroscopy titration of *sinIR*. Six titration curves were produced for every DNA target, and two of six titration curves for *sinIR* are shown here for clarity. For each titration, the concentration of protein titrated ranged 1 order of magnitude on either side of the previously reported or expected K_d and the DNA concentration was kept at the previously reported or expected K_d. Subsequently for each DNA target, six titration curves were globally fit to eq 1. Then the resulting six K_d values for each DNA target were averaged and are listed in Table 3.

Table 4: Intrinsic DNA Parameters[a] for the Oligonucleotides Used in AbrB and AbrBN Binding Studies

promoter	minor groove width (Å)	stretch (deg)	opening (deg)	propeller twist (deg)
sinIR	6.1	−0.107	−6.40	0.139
spo0E	5.2	−0.095	−6.79	0.158
BS18	5.2	−0.108	−6.36	0.136
TGGNA1	7.1	−0.103	−6.52	0.145
TGGNA3	4.7	−0.103	−6.49	0.141
all known natural binders	4.6−7.4	−0.108 to −0.087	−6.32 to −7.18	0.132−0.172
negative control	4.0	−0.121	−5.90	0.115

[a] The table shows the trend for several parameters for the modeled DNA. All modeling of each sequence was carried out on B-DNA. This table lists those parameters that are essential in deducing the strength of DNA−protein interactions.

in both positive and negative ion modes. In the positive mode, the affinity of the DNA and protein−DNA complexes for cations present in solution formed salt adducts which results in adversely broadened peaks in the μESI-MS spectra. While both positive and negative ion modes afford signals that could be easily assigned and deconvoluted, the negative ion mode was chosen because of less salt adduct formation and the corresponding improved spectral quality. In the negative ion mode, the DNA spectra generated both single-stranded and double-stranded DNA ion series. Deconvolution of these data provided the correct molecular mass for all the expected values of the DNA sequences (data not shown). All protein−DNA complexes were stable over time and under conditions of increased electrospray ionization voltage and capillary temperatures.

μESI-MS experiments revealed that the multimeric state of AbrB is a tetramer unbound and bound to all DNA in

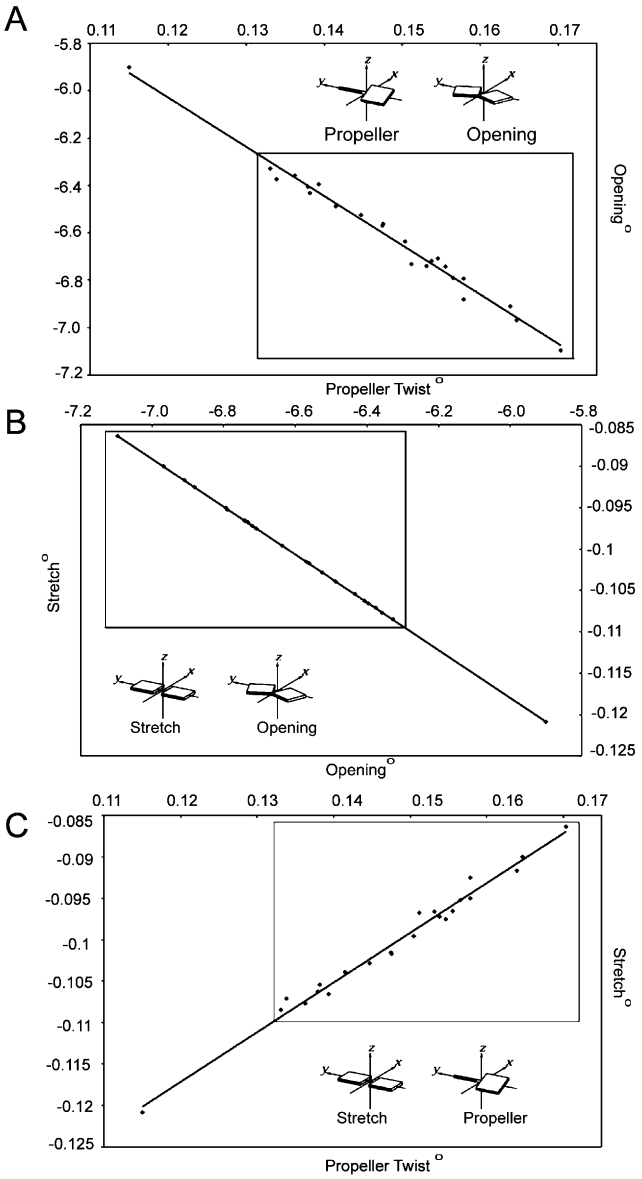

FIGURE 8: Molecular modeling of DNA binding targets of AbrB. The program 3DNA was used to examine more than 22 different local DNA structural parameters based on di- and trinucleotide steps. DNA PDB entries made through MODELIT were constructed as bent and straight B-DNA, energy-minimized through AMBER. Three DNA structural parameters showed relationships similar to that of the relative binding affinity seen in μESI-MS, CD, fluorescence, and UV spectroscopy: (A) propeller twist vs opening, (B) stretch vs opening, and (C) stretch vs propeller twist. The data contained inside the box are for the binding targets, and the one outlier corresponds to the negative control (nonbinder).

this and previous studies (Figures 1 and 2) (*8*, *19*). While we cannot rule out through μESI-MS alone that a small equilibrium exists between monomeric, dimeric, and tetrameric AbrB, we do not observe monomeric or dimeric species in the ESI-MS spectra of AbrB−DNA complexes. This strongly suggests that only the tetrameric form of AbrB is functionally significant (*31*, *37*, *38*). Additionally, SELC and native gel electrophoresis studies have shown only tetrameric AbrB to be present in solution, with no evidence for dimeric or monomeric forms (*19*, *21*, *30*). Other studies have accurately and quantitatively determined by ESI-MS that solution-based, dissociation-based processes are preserved (*26*, *39*). With this in mind, it appears that for the

case of AbrB any equilibrium among monomeric, dimeric, and tetrameric forms is negligible (*8*). In addition, no complex was seen with the negative control. AbrBN is seen to bind solely as a dimer to the same DNA used in the titrations with full-length AbrB and maintains the same dimeric state in the unbound form (Figures 1 and 3). The negative control afforded no complex and thus provided a reasonable baseline for assessing sequence specificity interactions between AbrB, AbrBN, and the DNA targets. Importantly, the results using AbrBN also confirmed that determinants responsible for binding DNA reside entirely within the N-terminal domain. The N-terminal domain thus represents the apparent minimal structural requirement necessary to bind DNA *in vitro*. The collected spectra showed the ability of AbrB and AbrBN to bind and form stable and significant/relevant complexes with the DNA oligonucleotides used in this study (Figures 2 and 3). The spectra also provided information concerning the relative affinity of AbrB and AbrBN for DNA. Charge state envelopes shifted to higher *m*/*z* values upon incubation of protein and DNA (as compared to protein alone), an indication of complex formation.

For all the μESI-MS spectra that were obtained, the same concentrations of individual protein, DNA, and buffer were used and each complex was analyzed using identical μESI-MS conditions. μESI-MS spectra were obtained for each sample multiple times and displayed the same result of relative ion intensity level (within experimental error) for all complexes. DNA target sequences were predominantly designed to have similar ionization efficiencies so that the relative ion abundance μESI-MS spectra of the AbrB−DNA complexes could be directly compared. The shortest target sequence used was *sinIR* which possesses a slightly lower ionization efficiency in the negative ion mode. However, the AbrB−*sinIR* and AbrBN−*sinIR* complex peaks seen in Figures 2A and 3A, respectively, are substantially more intense than for all other complexes. This indicates that the interaction between AbrB and *sinIR* is even stronger than that suggested by direct comparison. Therefore, the relative affinity of complexes can be inferred in a straightforward manner (*23*, *26*, *31*, *37*, *40*−*42*). The highest-relative intensity signals from the protein−DNA interactions were observed for AbrB−*sinIR* and AbrBN−*sinIR* complexes. Conversely, for protein equilibrated with the negative control, there were no detectable species corresponding to the molecular mass of a protein−DNA complex (Figures 2 and 3). From these data, the DNA strength of binding can be ranked on the basis of the level of complex present in the following manner: *sinIR* ≫ *spo0E* > *BS18* > *TGGNA3* > *TGGNA1* ≫ negative control. The differences seen in the relative affinity of AbrB−DNA binding by μESI-MS prompted investigations of structural components of AbrB, AbrBN, and the DNA that could account for the binding disparity observed via μESI-MS. Additionally, these subsequent studies were also intended to endorse the use of μESI-MS for this type of analysis.

To investigate general conformational changes upon DNA binding, CD and tyrosine fluorescence emission were used to probe the structural characteristics of AbrB, AbrBN, and the DNA. CD was employed to discern any gross changes in structural motifs of AbrB, AbrBN, and the DNA that may contribute to this differential binding. While CD provided an excellent method of probing secondary structure, our studies were limited by instrumentation sensitivity. The lowest concentration that could be used to provide acceptable spectra was not within a range of calculated affinity constants. For this reason, CD was used only for structural characterization and quantitation of affinity constants was not pursued. While it is not possible to deconvolute the protein CD data into their secondary structural elements, reference spectra described by Baase and Johnson (*29*) indicate that the data for both AbrB and AbrBN are consistent with proteins that contain both α-helix and β-sheet elements, with the α-helical structures contributing to the minimum at 208 nm. The AbrB and AbrBN protein spectra are not superimposable when the data are normalized for the total number of amino acids for each protein. Analysis of the mean residue ellipticity suggests the secondary structure of the AbrBN dimer was affected by the loss of the C-terminus to some degree.

All spectra of unbound and bound DNA maintained characteristics of B-DNA throughout protein titrations (Figure 4). As AbrB bound each target, the intensity of the CD signal at ∼215 nm displayed the same trend in relative binding affinity as determined via μESI-MS. A DNA distortion difference plot was obtained from subtraction of the maximum intensities around ∼215 nm for each oligonucleotide from the intensity of the negative control in their unbound and bound state. Figure 4 also shows the level of DNA distortion is greatest in *sinIR* upon binding, but occurs in all DNA targets with the notable exception of the negative control (Figure 5). This is a particularly strong indication that no binding occurs at all between AbrB and the negative control (*3*). A particularly significant finding from CD studies was that the negative control is significantly more topologically constrained (blue shifted by 5.4 nm) compared to the other target sequences. The ability of a DNA target sequence to be able to easily alter its conformation is therefore critical in its ability to bind AbrB. This flexibility represents the first characteristic of DNA that has been determined to be a contributing factor in the ability of AbrB to bind its targets.

To ensure that the complexation, as seen in μESI-MS, does not require any ionic cofactor binding or that there is not any buffer-induced conformational change occurring, the titrations were repeated in the presence of $MgCl_2$ and in different buffers with variable pHs. In all instances, no differences were observed in the spectra that were obtained (data not shown). These data support our conclusions and develop previous suggestions that AbrB recognizes multiple/flexible conformations of DNA (*30*).

Tyrosine fluorescence emission is a very useful probe in characterizing the interactions of AbrB since the only tyrosines present in the protein, Y37 and Y48, are located in the N-terminal DNA-binding domain (AbrBN). The structure of AbrBN indicates that the two tyrosine residues reside in the β-sheet scaffold of the dimerization interface and are solvent-exposed (*10*, *11*). In addition, monitoring fluorescence differences between AbrB and AbrBN provides the first information about the orientation of the N-terminus with respect to the C-terminus. The relative fluorescence level decreased when AbrB was compared to AbrBN, approximately 2-fold. This is due to the ionic state of the exposed tyrosine residues in AbrBN compared to those in AbrB; both tyrosine residues in AbrBN are likely protonated as they are

solvent-exposed. One tyrosine in AbrB is most likely hydrogen bonded as a tyrosinate anion with a cation in the C-terminus of AbrB, thereby reducing the level of emission by half. This suggests, for the first time, that the C-terminus positions itself so that it contacts the β-sheet scaffold of the dimerization domain in AbrBN, thereby contributing to the loss of signal.

It was determined that varying pH, as well as the introduction of Mg^{2+} as a possible binding cofactor, did not affect the overall tyrosine emission spectra, suggesting no major conformational changes in the DNA (Figure 6A). This is comparable with μESI-MS and CD studies. Fluorescence was also used to probe protein−DNA interactions. Emission at 345 nm was normalized to the response from *sinIR*, which is seen to be the strongest binder in μESI-MS and CD studies. The resulting AbrB−DNA relative binding affinity hierarchy from the fluorescence data is identical to those provided by μESI-MS and CD studies: *sinIR* ≫ *spo0E* > *BS18* > *TGGNA3* > *TGGNA1* ≫ negative control (Figure 6B).

Though the relative AbrB−DNA binding trend was determined independently via three different spectroscopic techniques, solution phase dissociation constants have not been available to this point. In addition, the previously reported dissociation constants based on gel shift assays have been inconsistent (*3*, *21*, *34*). While the gel shift studies provide a reasonable approximation for affinity, they seem to be contradictory (Table 3). To address this, we used UV spectroscopy to determine solution phase dissociation constants. The results from these studies were subsequently used to reinforce the relative binding data obtained in the μESI-MS, CD, and tyrosine fluorescence emission experiments described here. Solution phase dissociation constants (Table 3) determined by UV spectroscopy showed that the following order of binding to AbrB determined by other methods is reasonable: *sinIR* ≫ *spo0E* > *BS18* > *TGGNA1* > *TGGNA3* ≫ negative control. The solution phase dissociation constants are in general agreement with those previously determined by gel shift assays but have the distinct advantage that they did not require separation of free and bound mixtures of protein and DNA that may perturb the equilibrium (*25*, *26*).

The four separate bioanalytical techniques used in this study provide some of the first detailed insights into both the promiscuity and specificity of AbrB−DNA binding. To supplement these studies, molecular modeling approaches were employed using the program 3DNA. 3DNA is a robust molecular modeling program capable of handling complex rebuilding routines to define local structural features of DNA (*28*). Molecular modeling provided a means of identifying DNA structural components and parameters that may be responsible for the discrimination and binding specificity of AbrB and perhaps transition state regulators as a class of proteins. The targets used in this study, along with all other known natural DNA targets of AbrB, were modeled (Table 2). Comparisons of the parameters that likely play a role in AbrB binding are given in Table 4. The molecular modeling studies determined that the DNA structural characteristics of propeller twist, opening, and stretch were similar for all the AbrB targets that were examined. Significantly, the nonbinding negative control DNA was predicted to possess structural characteristics that were notably different from those of all the binding targets (Figure 8). While the negative control is seen to lie considerably outside the range of values of propeller twist, opening, stretch, and minor groove width required for binding, more thorough studies on a larger, statistically more relevant group of targets need to be performed. Nevertheless, the modeling work described here lends definite credibility to the premise that AbrB interacts with a common three-dimensional DNA topology rather than a base-pairing consensus sequence. Molecular modeling provides a rapid technique that is suitable for the identification of the structural parameters found in AbrB binding sequences. Construction of potential binding and nonbinding sequences can be accomplished by specifically designing DNA molecules to fit the given subset of topological parameters unique to AbrB binding sequences. These predicted binding sequences can then be empirically verified for binding using μESI-MS to assess relative binding affinities and competitive binding behavior.

This comprehensive spectrometric, spectroscopic, and modeling study suggests a multitiered model for binding site discrimination and variable binding affinity which can begin to address the global regulatory properties of AbrB. An observable complex between AbrB and the negative control used in these studies did not form under any circumstances. This suggests that a dynamic condition, inherent to that sequence, is resistant to forming any type of stable or metastable complex, and any sequence approximating this conformation is rejected. This initial level of discrimination would be followed by a more rigorous sampling of potentially higher-affinity interaction sites based upon allowable ranges of structural parameters (minor groove width, propeller twist, opening, and stretch). Therefore, binding affinities will vary on the basis of the conformational flexibility presented to the protein. The variable affinities of binding may play a very important functional role. AbrB regulates a multitude of genes whose simultaneous expression would be extremely detrimental to the cell. Therefore, it is possible that a safer, temporal order for lifting the repressive effects of AbrB could be established by virtue of the observed differences in AbrB−DNA binding affinities (*10*, *17*). Environmental and metabolic factors can affect protein conformation and their ability to respond to stimuli. The same concept may be true for the gene targets of AbrB, where changing environmental conditions in the transition state could alter local DNA topology. These local changes in DNA could serve as signals to alter the affinity at the AbrB binding site and thus play an important regulatory role. Our studies show that several DNA structural characteristics are required for interaction with AbrB, and even minor perturbations in one or more of these characteristics could result in either a more pronounced binding event or a complete inability to bind.

In summary, several conclusions and propositions can be made on the basis of the work presented here. Overall, these studies are the first to identify and detail any specific DNA traits that contribute to AbrB's ability to bind to more than 60 DNA targets that share no base pair consensus sequence. Our investigations underscore the need for some conformational suppleness of the gene target region for AbrB−DNA binding to occur. All the known natural binding DNA targets of AbrB display a propensity or ability to alter conformation slightly upon binding, while the apparent rigidity of the negative control DNA sequence prevents it from binding to AbrB at all. It is then likely that a sustainable and significant

interaction between AbrB and one of its gene targets is the result of a combination of a set of DNA structural parameters falling within a defined range (e.g., propeller twist, opening, stretch, and minor groove length).

CD experiments provided a means of monitoring structural characteristics of the protein, DNA, and protein−DNA interactions. Fluorescence studies also provided the first insight into the contact location for the C-terminal domain with the DNA-binding N-terminal domain of AbrB. UV experiments were used to obtain solution phase dissociation constants which helped clarify previous AbrB−DNA binding results by reporting solution phase constants in a manner that does not require the separation of bound and free mixtures. The UV studies also corroborate the results of various relative binding affinity measurements using μESI-MS, CD, and fluorescence. Molecular modeling of AbrB's DNA targets provides the first insight into both shared and contrasting features that play a role in the promiscuity and discrimination traits involved in AbrB−DNA binding.

Of particular note is the fact that the CD and fluorescence studies discussed accurately confirmed the relative binding affinity hierarchy for AbrB−DNA interactions initially determined by μESI-MS: *sinIR* ≫ *spo0E* > *BS18* > *TGGNA3* > *TGGNA1* ≫ negative control. The CD and fluorescence studies, of course, took much longer to complete than the μESI-MS studies. This clear corroboration of using μESI-MS for determining the relative affinities of noncovalent interactions is an extremely valuable result. In principle, and with experimental care, μESI-MS binding studies can be of exceptional use in rapidly defining a hierarchy of relative binding for nearly any protein−ligand mixture. With all other experimental parameters being consistent, relative binding affinities can be obtained if the ionization potential of the ligand is taken into account. In this study, we have shown μESI-MS's ability to describe the relative binding affinities of the protein−DNA interaction between AbrB and its DNA targets when ionization potentials of the DNA were taken into consideration. It is apparent that using μESI-MS as a very rapid high-throughput assay to study relative interactions of DNA-binding proteins is both appealing and feasible (*43*).

ACKNOWLEDGMENT

We thank Douglas Kojetin and Daniel Sullivan in the Cavanagh lab for providing assistance and informative discussions with initial modeling studies.

REFERENCES

1. Sonenshein, A. L., Hoch, J. A., and Losick, R. (2002) *Bacillus subtilis and its closest relatives: From genes to cells*, ASM Press, Washington, DC.
2. Fisher, S. H., Strauch, M. A., Atkinson, M. R., and Wray, L. V., Jr. (1994) Modulation of *Bacillus subtilis* catabolite repression by transition state regulatory protein AbrB, *J. Bacteriol. 176*, 1903−1912.
3. Xu, K., and Strauch, M. A. (1996) In vitro selection of optimal AbrB-binding sites: Comparison to known in vivo sites indicates flexibility in AbrB binding and recognition of three-dimensional DNA structures, *Mol. Microbiol. 19*, 145−158.
4. Furbass, R., Gocht, M., Zuber, P., and Marahiel, M. A. (1991) Interaction of AbrB, a transcriptional regulator from *Bacillus subtilis* with the promoters of the transition state-activated genes tycA and spoVG, *Mol. Gen. Genet. 225*, 347−354.
5. Dubnau, D., Hahn, J., Roggiani, M., Piazza, F., and Weinrauch, Y. (1994) Two-component regulators and genetic competence in *Bacillus subtilis*, *Res. Microbiol. 145*, 403−411.
6. Bol, D. K., and Yasbin, R. E. (1994) Analysis of the dual regulatory mechanisms controlling expression of the vegetative catalase gene of *Bacillus subtilis*, *J. Bacteriol. 176*, 6744−6748.
7. Robertson, J. B., Gocht, M., Marahiel, M. A., and Zuber, P. (1989) AbrB, a regulator of gene expression in *Bacillus*, interacts with the transcription initiation regions of a sporulation gene and an antibiotic biosynthesis gene, *Proc. Natl. Acad. Sci. U.S.A. 86*, 8457−8461.
8. Cavanagh, J., Thompson, R., Bobay, B., Benson, L. M., and Naylor, S. (2002) Stoichiometries of protein−protein/DNA binding and conformational changes for the transition-state regulator AbrB measured by pseudo cell-size exclusion chromatography−mass spectrometry, *Biochemistry 41*, 7859−7865.
9. Vaughn, J. L., Feher, V., Naylor, S., Strauch, M. A., and Cavanagh, J. (2000) Novel DNA binding domain and genetic regulation model of *Bacillus subtilis* transition state regulator abrB, *Nat. Struct. Biol. 7*, 1139−1146.
10. Strauch, M. A., and Hoch, J. A. (1993) Transition-state regulators: Sentinels of *Bacillus subtilis* post-exponential gene expression, *Mol. Microbiol. 7*, 337−342.
11. Strauch, M. A., Wu, J. J., Jonas, R. H., and Hoch, J. A. (1993) A positive feedback loop controls transcription of the spoOF gene, a component of the sporulation phosphorelay in *Bacillus subtilis*, *Mol. Microbiol. 7*, 967−974.
12. Shafikhani, S. H., Mandic-Mulec, I., Strauch, M. A., Smith, I., and Leighton, T. (2002) Postexponential regulation of sin operon expression in *Bacillus subtilis*, *J. Bacteriol. 184*, 564−571.
13. Qian, Q., Lee, C. Y., Helmann, J. D., and Strauch, M. A. (2002) AbrB is a regulator of the σ(W) regulon in *Bacillus subtilis*, *FEMS Microbiol. Lett. 211*, 219−223.
14. Hamoen, L. W., Kausche, D., Marahiel, M. A., van Sinderen, D., Venema, G., and Serror, P. (2003) The *Bacillus subtilis* transition state regulator AbrB binds to the −35 promoter region of comK, *FEMS Microbiol. Lett. 218*, 299−304.
15. Saile, E., and Koehler, T. M. (2002) Control of anthrax toxin gene expression by the transition state regulator abrB, *J. Bacteriol. 184*, 370−380.
16. Koehler, T. M. (2002) *Bacillus anthracis* genetics and virulence gene regulation, *Curr. Top. Microbiol. Immunol. 271*, 143−164.
17. Vaughn, J. L., Feher, V. A., Bracken, C., and Cavanagh, J. (2001) The DNA-binding domain in the *Bacillus subtilis* transition-state regulator AbrB employs significant motion for promiscuous DNA recognition, *J. Mol. Biol. 305*, 429−439.
18. Strauch, M. A. (1995) AbrB modulates expression and catabolite repression of a *Bacillus subtilis* ribose transport operon, *J. Bacteriol. 177*, 6727−6731.
19. Benson, L. M., Vaughn, J. L., Strauch, M. A., Bobay, B. G., Thompson, R., Naylor, S., and Cavanagh, J. (2002) Macromolecular assembly of the transition state regulator AbrB in its unbound and complexed states probed by microelectrospray ionization mass spectrometry, *Anal. Biochem. 306*, 222−227.
20. Zheng, G., Yan, L. Z., Vederas, J. C., and Zuber, P. (1999) Genes of the sbo-alb locus of *Bacillus subtilis* are required for production of the antilisterial bacteriocin subtilosin, *J. Bacteriol. 181*, 7346−7355.
21. Strauch, M. A. (1995) In vitro binding affinity of the *Bacillus subtilis* AbrB protein to six different DNA target regions, *J. Bacteriol. 177*, 4532−4536.
22. Strauch, M. A. (1995) Delineation of AbrB-binding sites on the *Bacillus subtilis* spo0H, kinB, ftsAZ, and pbpE promoters and use of a derived homology to identify a previously unsuspected binding site in the bsuB1 methylase promote, *J. Bacteriol. 177*, 6999−7002.
23. Strauch, M. A., Spiegelman, G. B., Perego, M., Johnson, W. C., Burbulys, D., and Hoch, J. A. (1989) The transition state transcription regulator abrB of *Bacillus subtilis* is a DNA binding protein, *EMBO J. 8*, 1615−1621.
24. Slack, F. J., Mueller, J. P., Strauch, M. A., Mathiopoulos, C., and Sonenshein, A. L. (1991) Transcriptional regulation of a *Bacillus subtilis* dipeptide transport operon, *Mol. Microbiol. 5*, 1915−1925.
25. Hagmar, P., Bailey, M., Tong, G., Haralambidis, J., Sawyer, W. H., and Davidson, B. E. (1995) Synthesis and characterisation of fluorescent oligonucleotides. Effect of internal labelling on protein recognition, *Biochim. Biophys. Acta 1244*, 259−268.
26. Kapur, A., Beck, J. L., Brown, S. E., Dixon, N. E., and Sheil, M. M. (2002) Use of electrospray ionization mass spectrometry to

study binding interactions between a replication terminator protein and DNA, *Protein Sci. 11*, 147−157.
27. Munteanu, M. G., Vlahovicek, K., Parthasarathy, S., Simon, I., and Pongor, S. (1998) Rod models of DNA: Sequence-dependent anisotropic elastic modeling of local bending phenomena, *Trends Biochem. Sci. 23*, 341−347.
28. Lu, X. J., and Olson, W. K. (2003) 3DNA: A software package for the analysis, rebuilding and visualization of three-dimensional nucleic acid structures, *Nucleic Acids Res. 31*, 5108−5121.
29. Baase, W. A., and Johnson, W. C., Jr. (1979) Circular dichroism and DNA secondary structure, *Nucleic Acids Res. 6*, 797−814.
30. Strauch, M. A., and Ayazifar, M. (1995) Bent DNA is found in some, but not all, regions recognized by the *Bacillus subtilis* AbrB protein, *Mol. Gen. Genet. 246*, 756−760.
31. Loo, J. A. (1997) Studying noncovalent protein complexes by electrospray ionization mass spectrometry, *Mass Spectrom. Rev. 16*, 1−23.
32. Cantor, C. R., and Schimmel, P. R. (1980) *Biophysical chemistry*, W. H. Freeman, San Francisco.
33. Sprecher, C. A., Baase, W. A., and Johnson, W. C., Jr. (1979) Conformation and circular dichroism of DNA, *Biopolymers 18*, 1009−1019.
34. Xu, K., and Strauch, M. A. (2001) DNA-binding activity of amino-terminal domains of the *Bacillus subtilis* AbrB protein, *J. Bacteriol. 183*, 4094−4098.
35. Klein, W., Winkelmann, D., Hahn, M., Weber, T., and Marahiel, M. A. (2000) Molecular characterization of the transition state regulator AbrB from *Bacillus stearothermophilus*, *Biochim. Biophys. Acta 1493*, 82−90.
36. Cheatham, T. E., III, and Young, M. A. (2000) Molecular dynamics simulation of nucleic acids: Successes, limitations, and promise, *Biopolymers 56*, 232−256.
37. Veenstra, T. D. (1999) Electrospray ionization mass spectrometry: A promising new technique in the study of protein/DNA noncovalent complexes, *Biochem. Biophys. Res. Commun. 257*, 1−5.
38. Pramanik, B. N., Bartner, P. L., Mirza, U. A., Liu, Y. H., and Ganguly, A. K. (1998) Electrospray ionization mass spectrometry for the study of non-covalent complexes: An emerging technology, *J. Mass Spectrom. 33*, 911−920.
39. Jørgensen, T. J. D., Roepstorff, P., and Heck, A. J. R. (1998) Direct determination of solution binding constants for noncovalent complexes between bacterial cell wall peptide analogues and vancomycin group antibiotics by electrospray ionization mass spectrometry, *Anal. Chem. 70*, 4427−4432.
40. van Berkel, W. J., van den Heuvel, R. H., Versluis, C., and Heck, A. J. (2000) Detection of intact megaDalton protein assemblies of vanillyl-alcohol oxidase by mass spectrometry, *Protein Sci. 9*, 435−439.
41. Tito, M. A., Miller, J., Walker, N., Griffin, K. F., Williamson, E. D., Despeyroux-Hill, D., Titball, R. W., and Robinson, C. V. (2001) Probing molecular interactions in intact antibody: Antigen complexes, an electrospray time-of-flight mass spectrometry approach, *Biophys. J. 81*, 3503−3509.
42. Elviri, L., Zagnoni, I., Careri, M., Cavazzini, D., and Rossi, G. L. (2001) Non-covalent binding of endogenous ligands to recombinant cellular retinol-binding proteins studied by mass spectrometric techniques, *Rapid Commun. Mass Spectrom. 15*, 2186−2192.
43. Benson, L. M., Kumar, R., Cavanagh, J., and Naylor, S. (2003) Protein-metal ion interactions, stoichiometries and relative affinities determined by on-line size exclusion gel filtration mass spectrometry, *Rapid Commun. Mass Spectrom. 17*, 267−271.

BI048399H